

# Metastability in Dark Current Diode Characteristics of Chalcogenide Photovoltaic Modules

Bettina Friedel

While present trends in commercial photovoltaic (PV) are set on a-Si/c-Si heterojunctions and promising perovskites, the chalcogenides still attract interest as an excellent candidate for coming multi- and heterojunction devices with perovskites. Continuously enhanced over the years, typical metastabilities in thin-film devices still cause issues under outdoor operation. Unfortunately, qualitative assessment in commercial PV is solely focused on data at the maximum power point of its operation, whether in simple on-site PV plant monitoring or following latest standards for certified laboratory testing, thus metastabilities merely register as undefined power fluctuations. Herein, it is shown that dark current characteristics are a simple and yet field-fit method, to identify metastable changes and take suitable counter measures. With this study, using commercial CdTe and CIGS showcase modules of various manufacturers and production generations, it is demonstrated how dark current characteristics allow to pinpoint physical changes of the individual module, between its pristine state, outdoor operation, dark degradation, and stabilization, like a fingerprint. Using the two-diode model, it is shown that alterations to respective regimes of the characteristic can be assigned to typical defects, defining the module's current state, and be used to it as a guide to evaluate its recuperation via preconditioning treatments.


## 1. Introduction

Metastability in thin-film photovoltaic (PV) devices is a remaining challenge in their commercialization, whether in established chalcogenides, new a-Si/c-Si heterojunctions, or the upcoming perovskites. Metastability thereby is simply a result of the character and deposition of the respective absorber materials. Being a polycrystalline thin film, surface-related defects and ion migration along grain boundaries will always dominate over those properties of the bulk semiconductor, and thus be prone to promote trap-assisted Shockley–Read–Hall recombination and

leakage pathways.<sup>[1,2]</sup> While these are omnipresent effects in thin-film PV, more technology-specific phenomena have to be considered as well. For instance, an effect referred to as “electronic doping” is typically seen in chalcogenide PV devices. Both CIGS and CdTe are p-type semiconductors, i.e., the second component to an operational p–n junction must be n-type. CdS, a wide bandgap semiconductor, fulfilled this role in older generation modules, but its deep defect levels cause its nature to change from n-type under illumination to p-type in the dark and vice versa. Therewith the superposition principle of dark current and photocurrent is not valid for chalcogenide PV, instead their recombination currents depend significantly on light intensity, spectrum, and bias.<sup>[3]</sup> CdS has been replaced by alternative semiconductors nowadays to reduce the problem. Another characteristic issue of chalcogenide devices is the energetic mismatch between the semiconductor and the back electrode due to the limited availability of

metals with suitable work function, like between CIGS and molybdenum.<sup>[4]</sup> In CdTe devices, Cu was traditionally used to form an ohmic contact toward the metal via Cu<sub>x</sub>Te<sub>1-x</sub> phases and as a beneficial dopant. Drawback of that strategy is the fast diffusion of Cu along lattice defects, migrating toward grain boundaries and layer interfaces, creating recombination centers and leakage pathways, while its depletion at the back contact again leads to an energy barrier.<sup>[5]</sup> Depending on their nature, the activation, promotion, or reversion of aforementioned metastability depends on illumination, bias, darkness, or temperature, rendering their behavior less predictable than that of classic wafer-based technologies. In commercial module testing, such effects are supposed to be compensated by mandatory stabilizing “preconditioning” procedures. Thereby technology-specific recipes, defining illumination dosages, duration, and stability criteria, are used to bring a module's power at the maximum power point ( $P_{MPP}$ ) to a stable maximum, before real characterization. However, despite specially adapted protocols, e.g., for CdTe as found in IEC 61215-1-2<sup>[6]</sup> and CIGS as found in IEC 61215-1-4,<sup>[7]</sup> that “stable state” is quite temporary and the  $P_{MPP}$  alone not qualified to define the modules momentary state or prove the recovery of earlier degradation effects. Occasionally, like in warranty cases, it might even be disadvantageous to blindly aim for a module's best  $P_{MPP}$ , when it was actually necessary to reinstate a particular previous state of performance to

B. Friedel  
Department 4.5 Applied Radiometry  
Physikalisch-Technische Bundesanstalt (PTB)  
Bundesallee 100, 38116 Braunschweig, Germany  
E-mail: bettina.friedel@ptb.de

 The ORCID identification number(s) for the author(s) of this article can be found under <https://doi.org/10.1002/pssr.202300239>.

© 2024 The Authors. physica status solidi (RRL) Rapid Research Letters published by Wiley-VCH GmbH. This is an open access article under the terms of the Creative Commons Attribution License, which permits use, distribution and reproduction in any medium, provided the original work is properly cited.

DOI: 10.1002/pssr.202300239

prove, e.g., climate-related underperformance at a plant, instead. The solution to this problem is the introduction of another marker besides the  $P_{MPP}$ , which can be used to define and adjust a module's condition, should be applicable on-site in the field and as insensitive as possible to outdoor fluctuations. The appropriate tool for that purpose is the dark current characteristic. Utilization of dark current characteristics is standard in solar cell research to analyze their device physics, ideal to unveil failure and loss mechanisms.<sup>[8]</sup> Unfortunately, the day-to-day testing in the module sector is dominated by power monitoring and thus the potential of dark IVs beyond research purposes is underrated, i.e., limited to special cases, like module development, stress testing, or in outdoor/plant research studies.<sup>[9]</sup> Analogously to a solar cell, the dark current behavior of a module can also be described by an appropriate equivalent circuit model. A module is basically construction of a number of serially connected cells, organized in parallel strings, and its current-voltage response is a superposition of the same. **In the case of thin-film cells and modules, the best way to represent them is by the two-diode model, i.e., an equivalent circuit comprising a main diode  $D_1$  representing the junction diffusion current, a secondary "weak" diode  $D_2$  representing recombination processes in the depletion zone and tunneling, a parallel shunt resistor  $R_{SH}$  representing parasitic leakage shunt pathways, and a resistor in series  $R_S$  representing bulk/interface/contact resistances and charge mobility.<sup>[10]</sup>** In special cases, e.g., Cu-rich CIGS, devices were reported to show nonohmic shunt contributions, which could not be fitted by the model as is. They were suggested to originate from imbalanced charge transport according to space-charge-limited current (SCLC) theory and compensated in the model by addition of a mobility-related power law term with parabolic voltage dependence.<sup>[11–13]</sup> In the present study, the two-diode model in its original form was sufficient to fit the data. The extended equivalent circuit for the two-diode model of a module is shown in **Figure 1**.

The corresponding two-diode equation for modules is

$$I = I_{01}N_p \left( e^{\frac{q \left( V - \frac{N_s}{N_p} I R_S \right)}{N_s n_1 k T}} \right) + I_{02}N_p \left( e^{\frac{q \left( V - \frac{N_s}{N_p} I R_S \right)}{N_s n_2 k T}} \right) + \frac{V - \frac{N_s}{N_p} I R_S}{\frac{N_s}{N_p} R_{SH}} \quad (1)$$

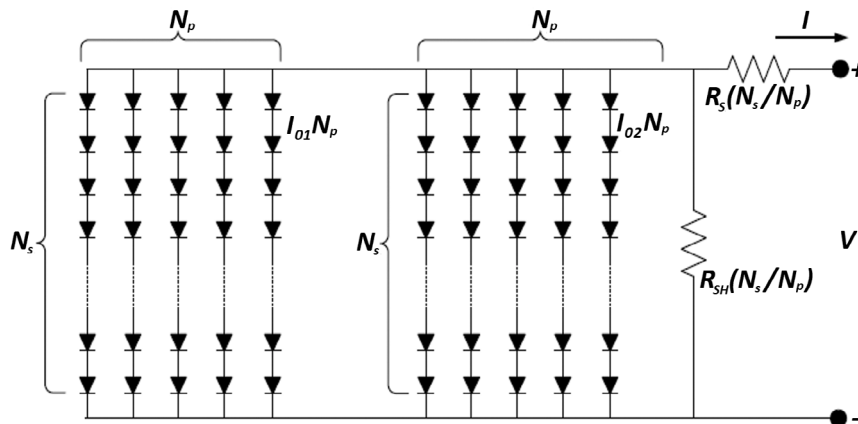


**Figure 1.** Equivalent circuit two-diode model for a PV module in the dark models.

Here, the respective diode's saturation currents are  $I_{01}$  and  $I_{02}$ , the ideality factors are  $n_1$  and  $n_2$ , the series resistance is  $R_S$ , and the shunt resistance is  $R_{SH}$ .<sup>[10]</sup> Further included are the numbers of modules in series  $N_S$  and of parallel strings  $N_P$ . **While for most cell types, the diode ideality factors of the two diodes are  $n_1 = 1$  and  $1 < n_2 < 2$ , they have been observed to be rather  $n_2 > 2$  in CdTe and CIGS devices due to their large density of traps.<sup>[4,12,14]</sup>**  $R_{SH}$  in CdTe and CIGS devices is mostly affected by pinholes and unwanted conductivity along the grain boundaries from metal migration, and can vary by two to three orders of magnitude even from module to module.<sup>[11,12,15]</sup> To gain these parameters, the module's current voltage data have to be fitted to the implicit two-diode equation, by an analytical, numerical deterministic or numerical stochastic approach.<sup>[16]</sup> An analytical solution requires considerable simplifications and partial solutions for sampling points (usually from photo IVs); therefore, the numerical way is simpler, but depends crucially on the careful setting of parameter boundaries. As this is quite challenging and time-consuming, the first sensible approach is a qualitative evaluation of cell/module dark current characteristics, by dividing the semilogarithmically curve visually into four different regions to analyze 1) the symmetric pit of the shunt resistance-dominated regime at low bias, followed by two successive linear regions of different slope, designated to 2) the "weak" recombination diode-dominated regime at low intermediate bias and 3) the "ideal" diffusion-dominated regime at higher intermediate bias, and finally the saturation of 4) the series resistance-dominated regime at high bias.<sup>[5]</sup> Where a distinction between the two diode regions is not possible, they should be treated as one, according to the one-diode model.<sup>[17]</sup>

In the present study, we demonstrate how a metastable PV module's dark current characteristic can be used as a fingerprint to track its change of state, by following typical alterations in those selected IV regimes as a reaction to dark degradation and outdoor operation, or inducing reversal of those alterations by preconditioning treatments of the module. Different to common mere monitoring of the module's maximum power  $P_{MPP}$ , dark IVs thus could provide an additional tool toward a potential new enhanced standard in commercial module stabilization and assessment.

## 2. Results and Discussion

### 2.1. Basic Properties of the Test Modules

As showcase modules in this study, we used a selection of chalcogenide modules, varying by type, technical generation, manufacturing method, and location, namely, CdTe module models FS-262, FS-265, and FS-4117A by First Solar, and CI(G)S module models WSG0074E063 from Würth Solar and SF-165 from Solar Frontier (for details, see Experimental Section). An initial dark current characterization has been done on all modules to identify technically induced differences between models and pristine defect/aging-induced module-to-module variations. **Figure 2** shows the initial dark current characteristics of five test modules per model of FS-262 (a), FS-265 (b), FS-4117A (c), WSG0074 (d), and SF-165 (e). The spectral response in terms of the external quantum efficiency (EQE) of a module of each model is also presented in Figure 2e.

The current–voltage (*IV*) characteristics have been plotted semilogarithmically for better visualization of the characteristic regions of the curve, which are indicated by dotted lines and labeled accordingly with  $R_{SH}$ ,  $D_2|D_1$ , and  $R_S$ . For the CdTe models (a–c), the dark current characteristics agree very well with the two-diode model, with clearly distinct regions of operation, especially for the two old models FS-262 and FS-265, where also the series resistance-dominated saturation region is within the measurable current limit. Except for three modules of the FS-265 model, none of the CdTe modules shows potential SCLC-related asymmetric nonohmic contributions in the shunt region. The distortions therefore originate most likely from isolated cases

of progressed degradation and are not a typical feature of CdTe modules. The shunt current among the tested modules within one batch always varies, in the case of model FS-262 even up to one order of magnitude with  $10^{-4}$ – $10^{-3}$  A @  $-30$  V, apparently due to generally higher density of shunting defects. For the other models, shunt currents are lower and scatter less around  $10^{-5}$  A @  $-30$  V. In the diode-dominated region, the modules of old generation CdTe models all vary in diode ideality (slope) and the saturation current (shift), suggesting different stages of degradation among the aged modules in one batch, e.g., by dopant diffusion. This is different for the new model FS-4117A, where only the “weak” diode ( $D_2$ ) regime varies from module to module, while the main diode’s ( $D_1$ ) behavior is identical. Looking at the series resistance-dominated region for the two old models FS-262 and FS-265, we also see slight variations from module to module, also suggesting dopant diffusion or interface degradation as the origin. Different to the CdTe modules under test, both CIGS models, WSG0074 and SF-165, have a bypass diode, impeding the analysis of reverse bias dark current to analyze symmetry in the  $R_{SH}$  region for potential SCLC effects, as can be seen in Figure 2c,d. **Quantitatively, shunt currents of the old WSG0074 model are relatively high, but exceptionally consistent across all modules within the batch, with around  $10^{-3}$  A @  $+10$  V.** For SF-165 on the other hand, there is a significant module-to-module variation between  $10^{-3}$ – $10^{-2}$  A @  $+30$  V. In the diode-dominated region, both CIGS models show only subtle variations of the slope between modules, compared to the CdTe models, and more pronounced for WSG0074 than SF-165.

As mentioned before, CdS is known to be responsible for a large range of reversible and irreversible degradation

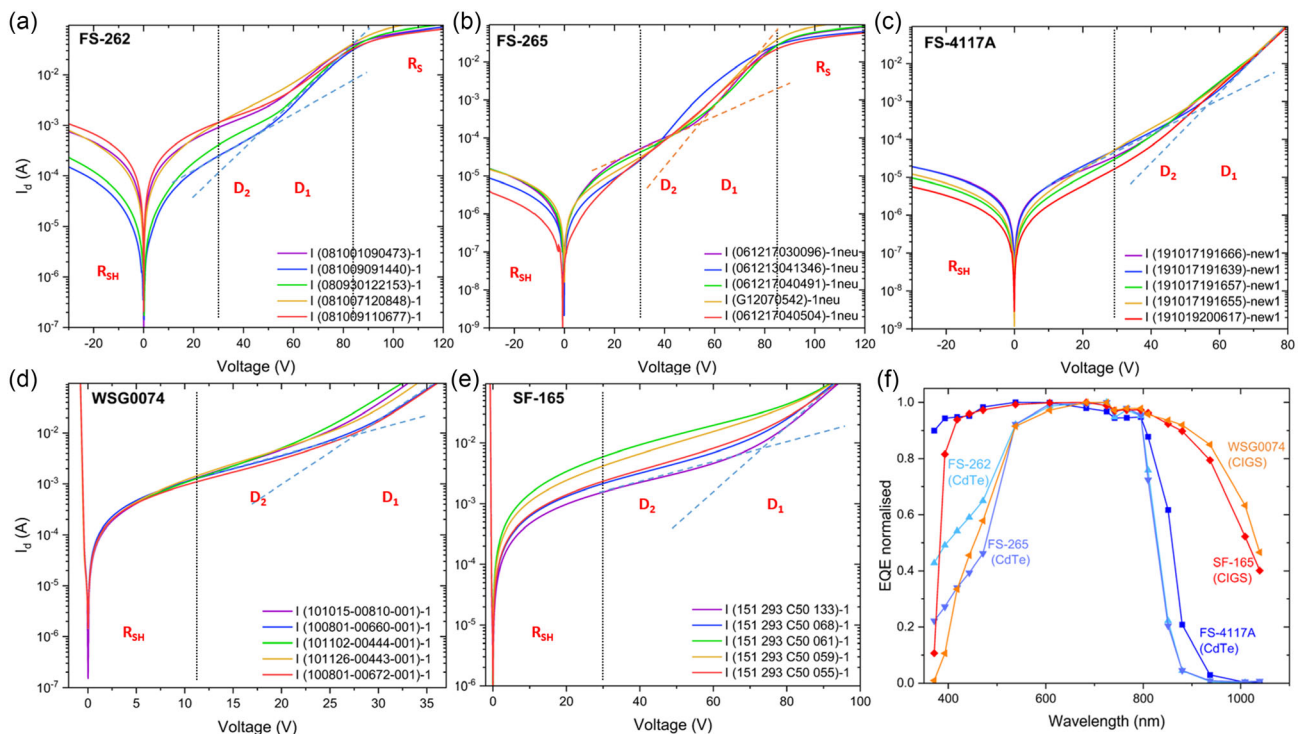


**Figure 2.** Basic dark current characteristic of all CdTe test modules of types a) FS-262, b) FS-265, and c) FS-4117, and of all CIGS test modules of type d) WSG0074-E063 and e) SF-165. f) Diagram shows the normalized EQE for the test modules.



phenomena in both CdTe and CIGS modules. Due to that fact, it has been reduced or replaced during technical advancement. CdS causes absorption losses in the blue spectrum; therefore, the measured spectral response of a module can tell whether it contains a CdS window layer or not. The EQE of all tested models (Figure 2f) shows expected broad featureless spectra, for CdTe typically narrower with no contributions beyond 900 nm and for CIGS going up to 1100 nm. On the short wavelength flank of the EQE, only the older module models of CdTe and CIGS show a shoulder in the spectrum, which is absent in the new models. This shoulder originates from parasitic absorption of CdS in those modules.<sup>[18]</sup> This confirms that CdS-related metastabilities should not occur in the new generation models.

Whereas the differences in the dark current characteristic between models can be easily explained by their type (CdTe vs CIGS), their architecture (with vs without CdS), and common aging, the significant module-to-module variations that were discovered within batches require more discussion. Different than wafer-based technologies, the nature of polycrystalline chalcogenide semiconductors and their deposition process provides several potential sources for variation. Typical for this technology are macroscale spatial inhomogeneities (e.g., thickness variations, nonuniform CdCl<sub>2</sub> posttreatment) on the one hand, and distributions of microscale defects on the other hand, such as pinholes, nonpassivated grain boundaries, or “microcraters.”<sup>[5,11,12]</sup> All investigated models show module-to-module variations in the weak diode regime, which is likely caused by spatial fluctuations of semiconductor thickness or inhomogeneities in dopant distribution, therewith is a normal feature of accordingly processed thin-film modules. The module-to-module variation in the main diode behavior and series resistance, which was only found for the older CdTe models, suggests additional cell-level degradation, such as interfacial blocking behavior at electrodes or changes charge mobility of the semiconductor by Cu migration or CdS-related effects, but possibly also from the module level, e.g., contact degradation, which is hard to distinguish at this point. The differences within one batch are probably due to the modules’ dissimilar treatment or storage before this study.

However, the most prominent observed module-to-module variation is the shunt resistance, regardless of type and age, which again suggests a manufacturing-based origin, like defects in the thin film. A visual inspection of the modules found indeed a range of even macroscopically visible imperfections, as shown in Figure 3. The images show small sections of interest (<5 cm) of various modules. The straight lines in all are the laser scribes between the cells. Defect features underneath the front glass are highlighted by arrows.

One feature that is found on all CdTe and on older CIGS modules is a white circular island defect of 1–2 mm diameter size, either formed around a larger white (Figure 3a) or dark particle (Figure 3c); others have a hole in their center (Figure 3d). Models FS-262 and FS-265 show the highest density of this defect type. Another less common feature, small (<1 mm) copper-colored exclusions, is only found on modules of the CdTe FS-262 series (Figure 3b). Much larger inhomogeneities (up to 30 cm) in the shape of grey streaks or clouded areas is found only on the CIGS modules WSG0074 (Figure 3e) and SF-165 (Figure 3f). Especially the small island defects are prone to cause microscopic

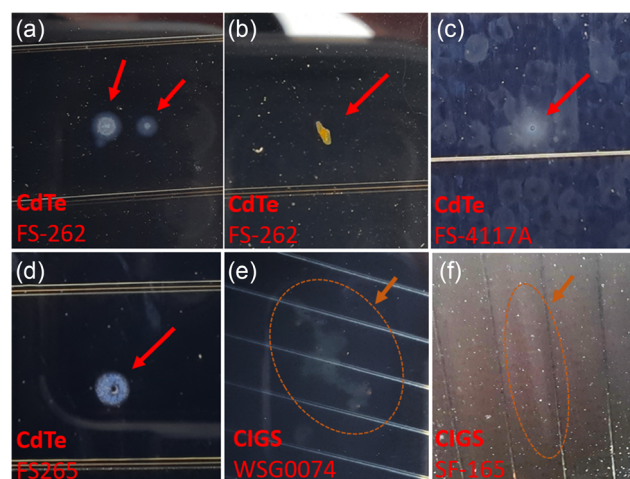


**Figure 3.** Photographs of different macroscopic defects on the a–d) CdTe and e–f) CIGS test modules.

short circuits, therewith lead to leakage currents in the respective cells and thus affect the shunt current of the entire module, depending on their scale and density. In consequence, also the weaker diode contribution increases.

From this initial evaluation of the test modules, we can conclude that the dark current characteristics show typical behavior associated with the cell-type (CdTe vs CIGS) and their cell architecture (e.g., CdS vs ZnO:Mg window, semiconductor composition), but additionally vary module-to-module due to overlaying effects from manufacturing-based inhomogeneities and differently progressed degradation effects from age/composition. This shows that the instantaneous dark current characteristic of a chalcogenide module is like a fingerprint of its type, quality, and state.

## 2.2. Long-Term Outdoor Operation

Due to their irradiance and temperature dependent metastabilities, the properties of chalcogenide modules change with the climate in their operating location and also even with the seasons.<sup>[19]</sup> Especially for a pristine “out-of-the-box” module, the season and climate of its first operation location is suspected to affect its achievable performance permanently for the future.<sup>[20]</sup> Metastable modules undergo changes during their outdoor exposure, with rates depending on spectrum, irradiance, and temperature. The common way to follow their performance development in the field is by monitoring of their output, i.e., the maximum power of the module. However, the analysis of these data can be tricky. Fast weather-caused fluctuations of irradiance and module temperature, even on nominally clear sky days with hardly noticeable high fog, cause the values to scatter even after irradiance–temperature (GT) correction to standard test condition (STC) and make visualization of a trend difficult. In the present study, the “out-of-the-box” test modules, i.e., after long period of dark storage, were installed outdoors (note: climatic region was Brunswick, Northern Germany) and their performance has been monitored over a period of 11 months (August–July),

covering all seasons. The recorded DC performance data were filtered down to clear sky days and midday hours. **Figure 4** shows the development of the STC-corrected  $P_{MPP}$ ,  $I_{MPP}$ , and  $V_{MPP}$  for our modules over this period.

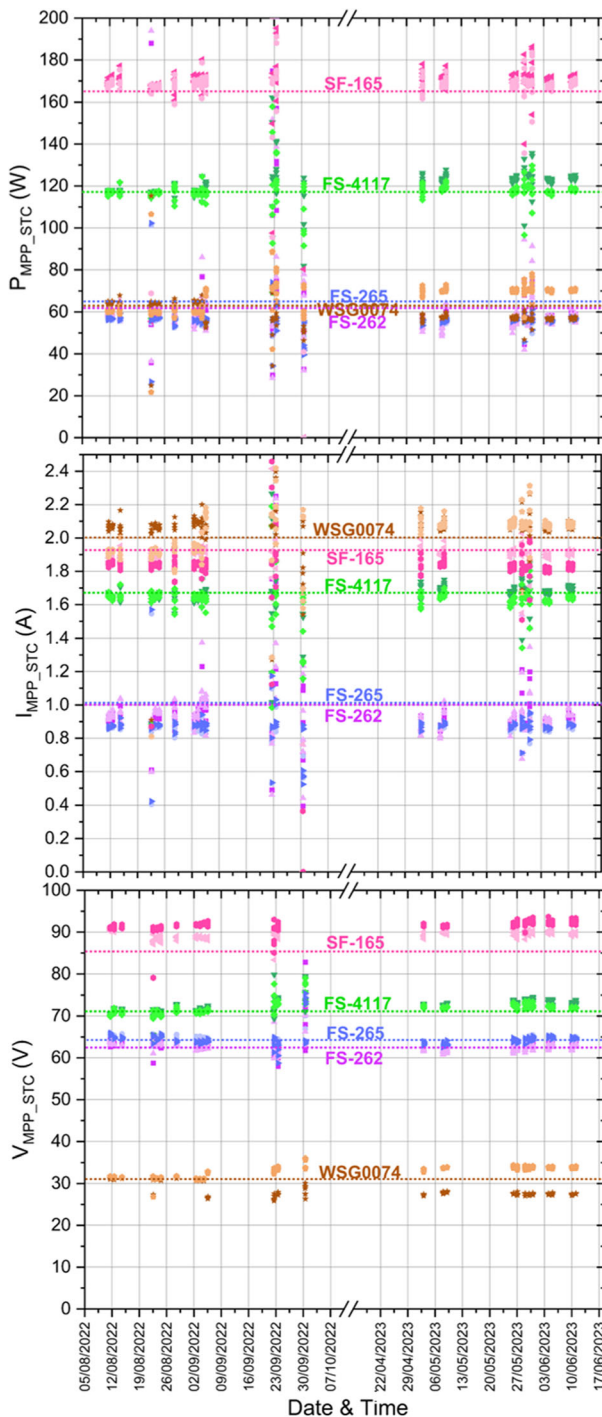


**Figure 4.** STC-corrected and filtered (clear sky days, midday hours) micro-inverter readings of  $P_{MPP}$ ,  $I_{MPP}$ , and  $V_{MPP}$ , of CdTe models FS-262, FS-265, and FS-4117A, and CIGS models WSG0074 and SF-165 (two modules each) over a period of 11 months. The respective label values are indicated with correspondingly colored dotted lines.

After filtering, only few datasets remain for summer, autumn, and spring months, none for winter. The scattering of the data is reduced significantly by GT correction (with few exceptions). According to the typical behavior of these module types, one would expect to see an increase in power and voltage during the first days of light exposure and also reduced performance after the winter break. Unfortunately, none of this is visible in the microinverter data for any of the models. Instead, power  $P_{MPP}$ , current  $I_{MPP}$ , and voltage  $V_{MPP}$  of the modules remain steady, irrespective of their type, model, or condition. This means either stabilization of the modules was already reached 2 days after installation, i.e., before the first useful datapoint was recorded, or these data are too imprecise to unveil subtle changes of the module performance. Interestingly, the new CIGS model SF-165 shows higher power than the label value, namely, 170 W instead of only 165 W and higher than specified voltage value  $V_{MPP}$ , with 90 V instead of 85 V. The old generation CdTe models FS-262 and FS-265 on the other hand are significantly underperforming, given their label power of 62.5 and 65.0 W, both stay below 60 W during operation, which is a result of their too low current, with merely 0.8–0.9 A where 1.0 A is expected for both. The other modules are close to their label values.

However, apparently stable outdoor DC performance values alone do not necessarily prove that the module did not change. In **Figure 5**, two exemplary sets of dark current characteristics for FS-262 CdTe modules are shown. The curves have been recorded at different points during the 11 months of outdoor operation (module temperature between 16 and 28 °C). The modules were measured in their initial “out-of-the-box” state (black curve) and then during outdoor operation after one day (purple), after 1 week (green), then again after the winter break in (yellow), in May (orange) and finally in August (red). Even with the unfortunate temperature-induced shift of the curves, there are reproducible changes in the module’s dark current behavior over the seasons. This is most pronounced in the series resistance-dominated current regime. While the module’s initial dark current characteristic shows high series resistance (indicated by the strong saturating curvature), just 24 h outdoors led to a tremendous decrease in series resistance (visible from the strongly reduced bending). One week later,  $R_s$  is further decreased. Interestingly, the first dark current characteristic after the winter break shows high series resistance again, meaning that the modules have degraded during winter with its seasonal lower irradiance, shorter day light, and mostly cloudy conditions. Over spring and summer, the modules recover again, showing repeated decrease in  $R_s$  in May and August.

These results demonstrate that dark current characteristics present a sensitive and versatile tool to complement standard outdoor monitoring to disclose changes in metastable modules.

### 2.3. Dark Degradation After Long-Term Outdoor Exposure

Before the application of dark current characteristics as a method to judge a PV module’s condition or stability in a standard, it should be verified that effects from dark degradation or module preconditioning can be recognized and quantified from them, irrespective of the module type or its condition. For that purpose, test modules of each model were placed in dark storage after

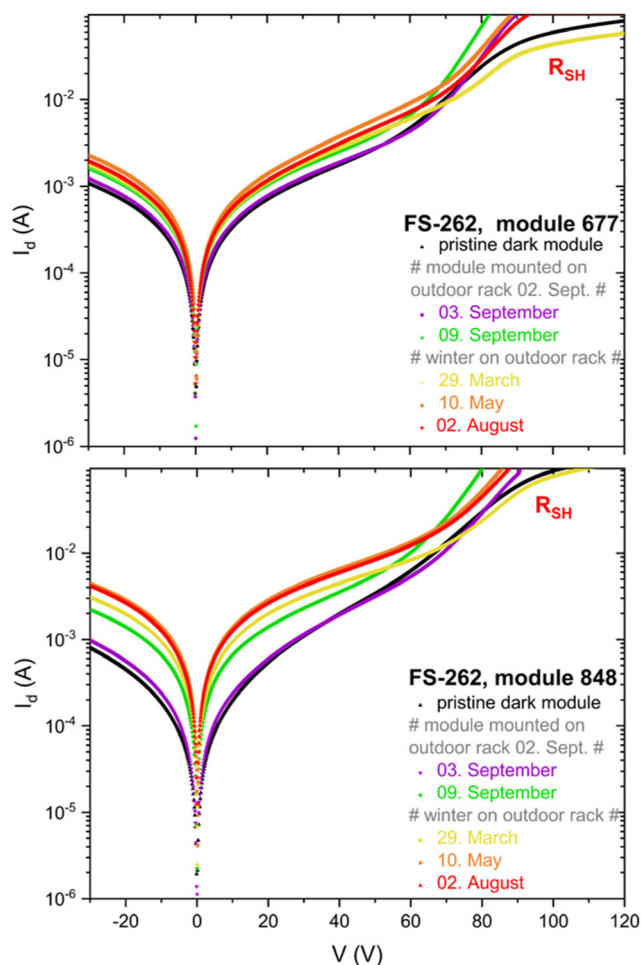


**Figure 5.** Dark current characteristics of two CdTe FS-262 modules of selected days over the seasons during their outdoor period.

6 months of outdoor operation (summer) and their dark current characteristics recorded regularly over the following 2 months, first hourly within the first 24 h and then with increasing time intervals, up to 1632 h. **Figure 6** shows the development of the dark current characteristics for each model during dark storage. The characteristics have again been divided into the four respective zones, dominated by shunts, recombination diode, diffusion diode, and series resistance. It can be clearly seen that dark degradation affects each of the modules in a slightly different way, but with a systematic pattern none the less. The old CdTe modules of series, FS-262 (Figure 6a) and FS-265 (Figure 6b), both react to the dark with a significant increase in series resistance, visible from the strong bending of the curve in the high bias region, just as observed during our seasonal outdoor observation.

Extraction of the  $R_s$  value from our numerical two-diode model fits confirms an increase from 1839 to 2828  $\Omega$  for FS-262, and from 1456 to 1761  $\Omega$  for FS-265, between 1 h and 1632 h of dark storage, respectively. Further, the slope of the curve in the “main” diffusion diode regime decreases with longer dark storage for both modules, indicating an increase of  $n_1$ . Our fits confirm  $n_1$  to increase from 280 to 294 and from 292 to 295, respectively. In the shunt and recombination-diode dominated

regions, the FS-265 module remains unaltered, while the FS-262 shows decreasing shunt current and a decrease of the diode ideality  $n_2$  of the recombination diode. Shunt pathways and recombination in that module appear to depopulated with longer dark storage. The fact that the FS-265 module does not show either must mean that it is generally in exceptionally good condition. The module of the FS-4117A series (Figure 6c) shows the same reaction to dark storage as FS-262, i.e., an increase in  $n_1$  in the diffusion regime, and the decrease of  $R_{SH}$  in combination with the decrease of the diode ideality of the recombination diode  $n_2$ . In the case of the CIGS models, the old WSG0074 module behaves very differently compared to the new SF-165 module. While the WSG0074 module (Figure 6d) shows merely a decreasing shunt current, it does not show simultaneous change of the recombination diode behavior, unlike the CdTe modules. The reason for this behavior is unclear. The SF-165 module, on the other hand (Figure 6e), shows the same trend as the CdTe modules FS-262 and FS-4117A, i.e., decrease in shunt current and recombination with longer dark storage. An interesting effect seen here is the omnipresent change of the diffusion diode behavior of CdTe upon dark degradation, which is completely absent in the CIGS modules. It can be assumed that the process might be associated with the copper diffusion from the back contact in CdTe devices, as this is the biggest difference between the two technologies. However, the underlying defect kinetics leading to this temporal dark degradation (sometimes also called “dark soaking” or “dark aging”) are still not entirely understood.<sup>[21]</sup> It can be concluded that the observed similar reaction of both technologies in the shunt and recombination regime can be explained by their joint typical features of pinholes and grain boundaries. These results agree well with reported observations for other polycrystalline solar cells with mixed contributions from bulk regions and grain-boundary regions.<sup>[2]</sup> Diminished leakage currents and reduced recombination for longer dark storage could indicate that the associated defects are less populated, which makes sense, as the saturation current of the recombination diode is directly related to the trap density and the charge carrier concentration.

#### 2.4. Illumination- and Bias-Induced Preconditioning

As dark degradation clearly affects the dark current characteristics of chalcogenide test modules, so should their recuperation if the effects are indeed reversible, as expected for a metastable module. Dark degradation in chalcogenide modules is suspected to be related to ion migration processes in the absence of an electric field, which can be reversed by exposing the module to its own  $V_{OC}$ ; therefore, the most prominent preconditioning treatment is illumination of the module.<sup>[22]</sup> However, other preconditioning methods, which have been tested thoroughly, are using bias and/or heat, often in combination with illumination.<sup>[23]</sup> This makes sense because if ion migration processes are the core problem of dark degradation, then an electric field with suitable direction to apply some driving force and heat to enhance ion mobility will accelerate the relocation of the ions. However, this only works if the ions are not trapped, like mentioned capture of  $\text{Cu}^{2+}$  by CdS in the dark. Therefore, illumination might be vital to activate the process by releasing the ions to begin with.



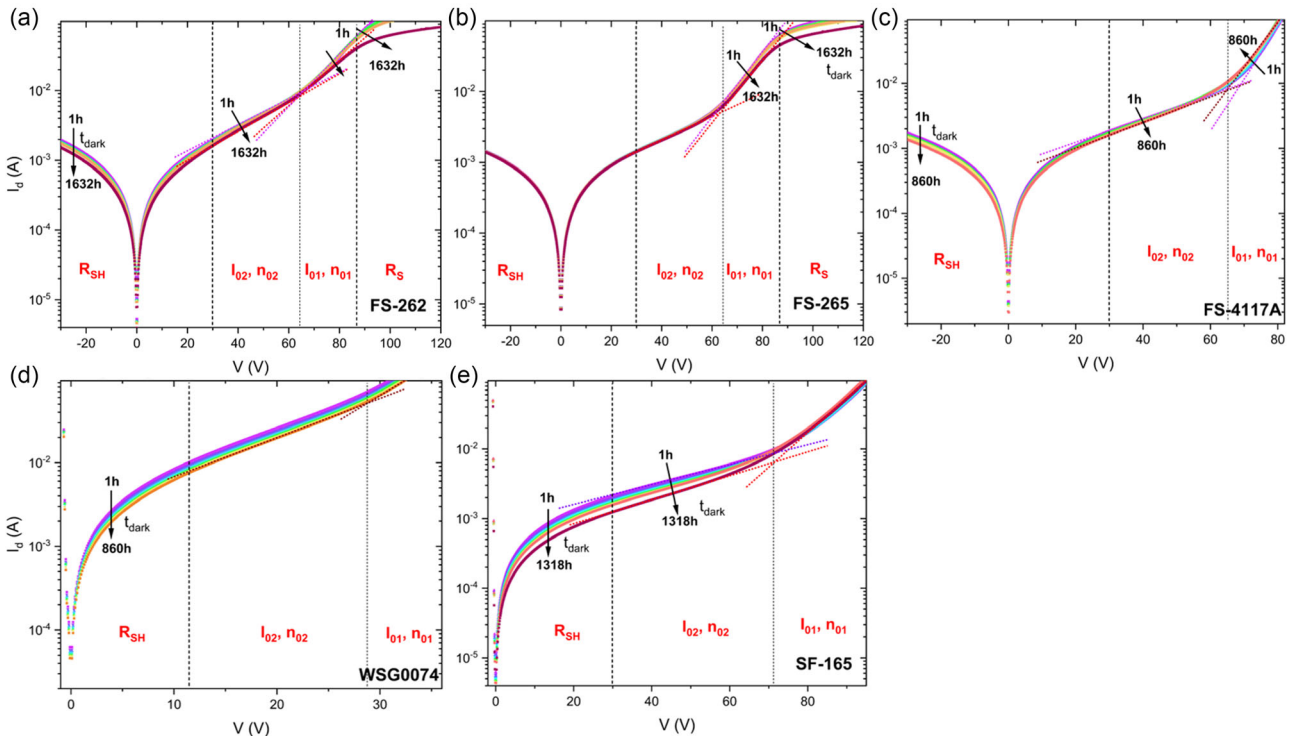


**Figure 6.** Development of the semilogarithmic dark current characteristics of all a–c) CdTe and d–e) CIGS test modules during 1–1632 h of dark storage after long-term outdoor operation. The regimes dominated by shunts, recombination, diffusion, and series resistance are labeled. Directions of change and broken lines along the linear diode contributions have been indicated as guide to the eye.

In another scenario, it might also be the larger current density during illuminated operation, which saturates dangling bonds and bulk defect traps and thus leads to recuperation of the device. In our preconditioning approach, we compare effects of short-term white light illumination and of forced forward bias sweeps in the dark on the dark IVs of dark-stored modules. By looking at their effects separately, one can distinguish which changes in the module behavior are illumination activated and which are not.

For illumination-induced preconditioning, modules from dark storage (3 months) were exposed to white light ( $850 \text{ W m}^{-2}$ ) for a period of 1 h. (Note: the modules were not the same ones as used during the dark degradation study, but of the same batch). The modules' dark current characteristics were recorded before the treatment and then directly after illumination (1 h to allow cooling to  $25^\circ\text{C}$ ) and then again in hourly intervals for up to 24 h, to study the dynamics of the illumination induced recuperation of the module. **Figure 7** shows the development of the dark IVs for the CdTe (Figure 7a–c) and CIGS (Figure 7d–e) test modules. The respective shunt, recombination, diffusion, and series resistance-dominated regions are indicated, where applicable. The illumination-induced shifts are highlighted by arrows for better visibility. The color coding (red–yellow–green–blue) marks the direction of relaxation of the illumination effect with longer time distance to the illumination.

The characteristics of the older FS-262 (Figure 7a) and FS-265 (Figure 7b) CdTe models demonstrate the module's reproducible development from the dark to the illuminated state and back, best of all models, due to the pronounced changes in the  $R_S$

regime. While dark storage causes substantial increase of  $R_S$  and an increase the diffusion diode's ideality factor  $n_1$ , short illumination successfully reverses the effect, as visible from the reduced curve bending at high bias and an increase of slope in the higher intermediate bias. Also, the development of shunt current and recombination are reversed by illumination. For the CIGS model WSG0074 (Figure 7d), the shunt current that decreased during dark storage recovers after illumination, too. Contrarily, for the new CIGS model SF-165 (Figure 7e), where dark degradation had led to an increase of  $R_{SH}$  and an increase in  $n_2$ , short illumination has only a very subtle reversing effect, suggesting that recovery rate is slower than for the other modules. These results show that the illumination-induced recovery of the modules can be monitored in the dark current characteristics and even conclusions on their recovery and degradation rates can be drawn.

To study how bias-induced preconditioning affects the chalco-genide modules' dark current characteristic, dark stored modules (3 months) were subjected to repeated slow ( $\approx 5 \text{ min}$ ) forward bias sweeps in the dark. This method was chosen above often suggested constant high voltage at elevated temperature because mild sweeps at moderate temperature are closer to the natural operating conditions of the modules and prevent unwanted material stress. The chosen voltage range was matched to the operating voltages of the modules, i.e., in a range from 0 to 120 V for all CdTe modules and the new CIGS module, and in a range from 0 to 45 V for the older CIGS module (slightly above  $V_{OC}$ ). **Figure 8** shows the bias-induced effects on the dark

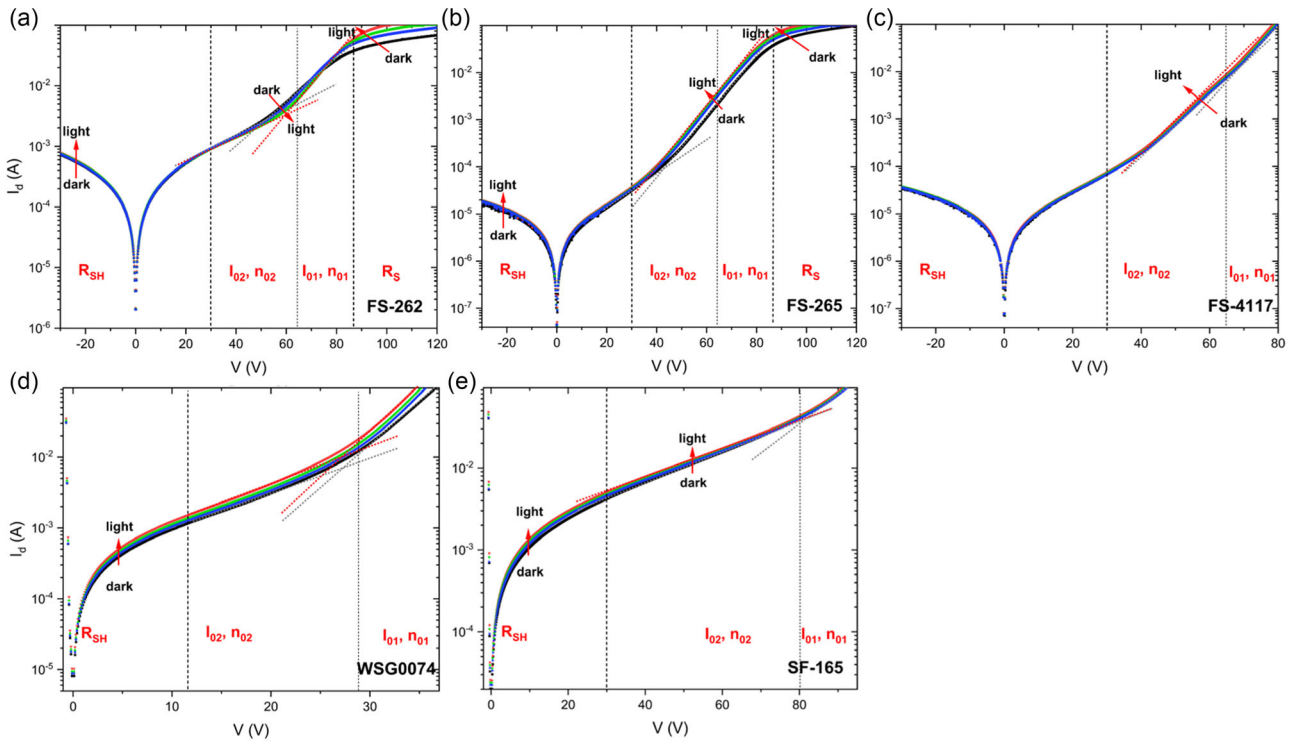


**Figure 7.** Illumination effects on different regimes of the semilogarithmic dark current characteristics of the CdTe models a) FS-262, b) FS-265, c) FS-4117A, and the CIGS models d) WSG0074 and e) SF-165. The shunt, recombination, diffusion, and series resistance-dominated regions are indicated. Directions of light-induced change are marked by the arrows.

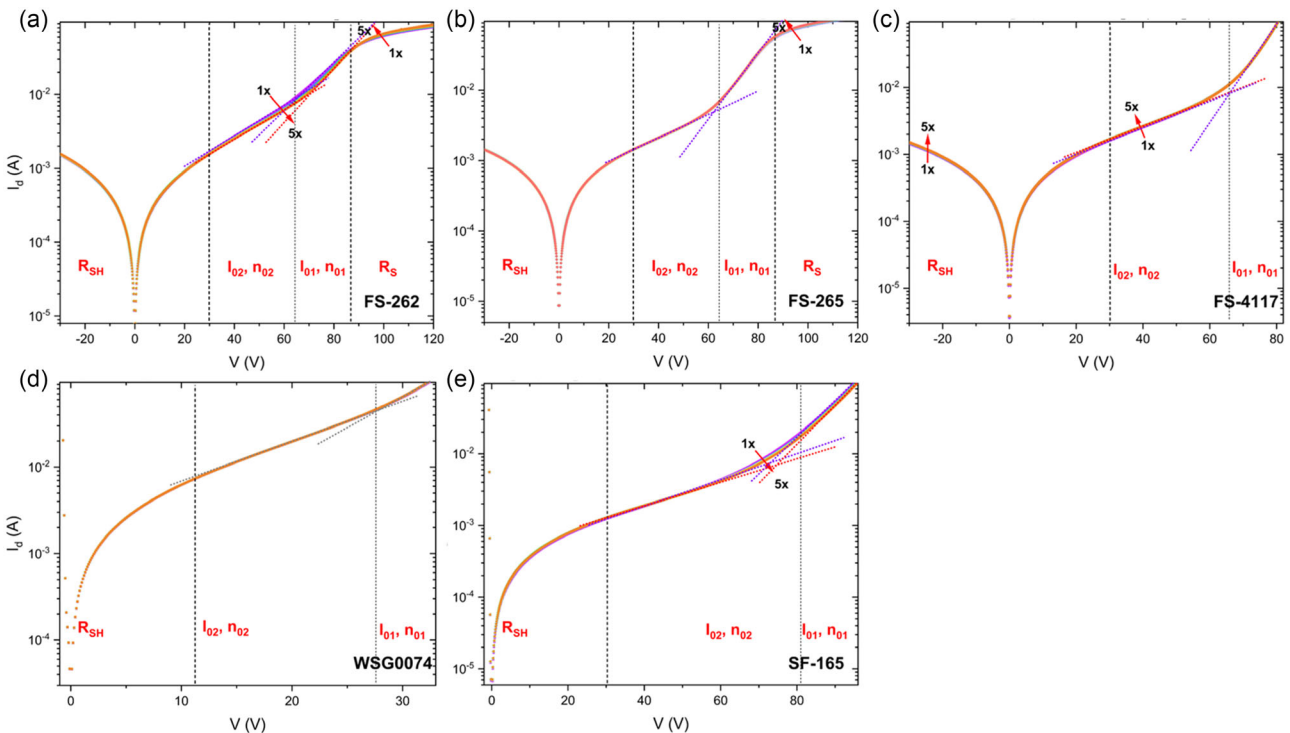


**Figure 8.** Effects of forward bias sweeps on the different regimes of semilogarithmic dark current characteristics for the CdTe test models a) FS-262, b) FS-265, c) FS-4117A, and the CIGS test models d) WSG0074 and e) SF-165. The shunt, recombination, diffusion, and series resistance-dominated regions are indicated. Directions of bias-induced change are marked by respective arrows.



current characteristics for the CdTe (Figure 8a–c) and of CIGS (Figure 8d–e) test modules. Again, the different current regimes are indicated. The trends of bias-induced changes are marked with an arrow in the direction of change. Most interestingly, the characteristics for all CdTe and CIGS models demonstrate that bias sweeps have almost no effect on the resistance-dominated regimes, neither the series resistance  $R_s$ , nor the shunt  $R_{sh}$ . Merely diode-related degradation effects were found to be reversed by bias sweeps, best visible from slope changes for FS-262 (Figure 8a) and SF-165 (Figure 8e), but only at a very low rate.

### 3. Conclusion

Reliable and accurate performance testing of metastable PV modules is challenging. Dark degradation occurs by change of environment, such as transport to a test lab or even by climate/season. Preconditioning, meant to stabilize the modules before testing, is presently focused merely on stabilizing their power at the maximum power point. Unfortunately, this value does not provide any information on the actual condition of the module, i.e., if a temporary degradation effect was compensated by preconditioning or if a module has been unintentionally altered in a completely different way. We suggested that dark current characteristics of modules could help to overcome this limitation. In a study of 25 chalcogenide modules of various types, age and manufacturer, we demonstrated that each module—even those within one batch—has an individual dark current characteristic that is like a fingerprint of its state. The partially significant module-to-module variations visible in dark IVs can be associated with their known defect types and production variations. Despite the fact that every module is slightly different, particular regions of the dark current characteristic exhibit distinct changes (shifts, slope changes, and bending of the curve) upon degradation in the dark and their reversal upon preconditioning by illumination. Also, tracking changes to the dark current curves during degradation or treatment allows to study the dynamics of either process and identify the origin. We further showed via dark current monitoring that bias-induced preconditioning in the absence of light or heat does only recover selected degradation effects, while being ineffective for others.

In combination with power monitoring, dark current characteristics would be a valuable tool for monitoring a module's condition during operation or treatment, using the dark IV as a guideline to reinstate a particular state (e.g., on-site of a PV plant) later after dark storage (e.g., transport to a test lab). This method could be used to develop stability time constants for metastable

modules, evaluate further preconditioning treatments, or assist with the development climate dependent label values for PV modules.

### 4. Experimental Section

**Sample Modules:** The showcase PV modules in this study were chalcogenide thin-film modules, thereby three different models of CdTe from First Solar and two different models of CI(G)S from Solar Frontier and from Würth Solar (see Table 1 for details).

Three different models of CdTe modules by First Solar have been chosen to account for technology advancements and for manufacturing variations between different production sites. The most significant difference between the FS-2 and FS-4 series is the replacement of CdS and the introduction of a graded Cd(Te,Se) layer to improve absorption and carrier life time. The two old First Solar models FS-262 and FS-265 are same generation but differ in production sites. This particular comparison is interesting because the Ohio plant (FS-265) was in the news when First Solar recalled an entire batch mid2008/mid2009, due to production issues. From the two models of CIGS, the new Solar Frontier model differs to the one older type by Würth Solar by the established enhancements of the cell composition, such as replacement of the CdS layer and introduction of graded absorber layer, additionally the difference of Solar Frontiers deposition two-step sputtering and selenization technique to Würth Solar's one-step coevaporation. For each model, five modules of consecutive serial numbers of the same production batch have been purchased where possible. The younger modules were in “out-of-the-box” condition, while older types were purchased second hand, but still officially labeled as “new/unused.” To account for some known history, unknown storage, and transport conditions, all modules were kept in dark storage within a climatic chamber at a temperature of  $<20^\circ\text{C}$  for 3 months before initial characterization.

**Methods:** Dark current characteristics of the modules were recorded with a Keithley 2612B system sourcemeter. Voltage sweeps were carried out in forward direction with measurement delay of 100 ms between voltage setting and current measurement. For dark storage and accompanying characterization, the modules were kept in complete darkness within fitted panel flightcases (ProfiPlus Screen FlexCase, by ProCase). For outdoor operation of the modules, they were mounted on a roof platform (16 m height) mounted to a  $37^\circ$  tilted rack facing southward. The modules were kept at maximum power point during operation by one AE-Conversion microinverter each. The inverter was chosen to fit the respective module's feed-in requirements, i.e., models INV350/60 for the Würth Solar modules and model INV500/90 for every other. The microinverters were connected to a datalogger, which recorded the modules'  $P_{MPP}$ ,  $V_{MPP}$ , and  $I_{MPP}$  values continuously with 1 min resolution. These data were  $G$ - $T$  corrected to STC (i.e.,  $1000\text{ W m}^{-2}$ , AM1.5G,  $25^\circ\text{C}$ ) via Standard Irradiance Desired Temperature procedure using the module's label temperature coefficients.<sup>[24]</sup> The irradiation  $G$  was logged in the module plane by a Mencke&Tegtmeier reference cell model Si-mV-85-Pt1000-4L-E. The temperature of the modules was measured by Omega-Engineering Pt100 thermosensors and recorded using a Graphtec midi-Logger GL840. For laboratory EQE measurements, a Wavelabs model SINUS-2100p module solar simulator (AAA+) served as the tunable light source. Thereby EQE was measured by a white-light-biased EQE approach, i.e., while under

**Table 1.** Models and specifications of showcase modules selected for dark degradation and preconditioning.

Model	Cell type	No. of cells	Production year/site	$P_{MPP\_STC}$ [W]	$I_{MPP\_STC}$ [A]	$V_{MPP\_STC}$ [V]
First Solar FS-262	CdTe, CdS	116	2008/Malaysia	62.5	1.00	62.5
First Solar FS-265	CdTe, CdS	116	2006/US	65.0	1.01	64.0
First Solar FS-4117 A-3	CdTe, ZnO:Mg	108 + 108	2019/Malaysia	117.5	1.68	70.1
Solar Frontier SF-165	CIS (Cu-In-Se/S), ZnS	74 + 74	2019/Japan	165.0	1.93	85.5
Würth Solar WSC0074063	CIGS (Cu-In-Ga-Se/S), CdS	66 + 66	2011/Germany	63.0	2.0	31.5

AM1.5G illumination, each of the 16 LED color channels is subsequently first over- and then undermodulated with respect to the AM1.5G spectrum and the respective wavelength-dependent  $I_{SC}$  extracted from the signal difference for each channel, resulting in an EQE curve with 16 wavelength points. White light preconditioning was either performed outdoors in sun light or in the lab with an LED-based large-area white light source with an irradiance of  $850 \text{ W m}^{-2}$ . Bias-based preconditioning was performed by repeated forward bias sweeps with a Keithley 2612B system sourcemeter. The sweep range was from 0 to 120 V for all models, except for Würth Solar's WSG0074 from 0 to 50 V. Each sweep duration (adjusted via holding time per voltage point) was 5 min. The dark current data were visually analyzed by dividing the semilogarithmically plotted characteristics into their respective dominated regimes of shunt resistance, recombination (diode 2), diffusion (diode 1), and series resistance. In some cases, data were fitted to the two-diode model to extract the model parameters. Therefore, the implicit formula was implemented in Python and fitted numerically to the measured data using the trust region method.

## Acknowledgements

B.F. is grateful for the financial support of the project "MetroKomPV" by the German Federal Ministry for Economic Affairs and Climate Action under the funding reference number: 03EE1024.

Open Access funding enabled and organized by Projekt DEAL.

## Conflict of Interest

The author declares no conflict of interest.

## Data Availability Statement

The data that support the findings of this study are available from the corresponding author upon reasonable request.

## Keywords

chalcogenide thin films, dark current characteristics, dark degradation, metastability, photovoltaic modules, preconditioning

Received: June 30, 2023

Revised: March 13, 2024

Published online: March 29, 2024

- [1] F. Greuter, G. Blatter, *Semicond. Sci. Technol.* **1990**, 5, 111.
- [2] K. Kurobe, H. Matsunami, *Jpn. J. Appl. Phys.* **2005**, 44, 8314.
- [3] a) G. Agostinelli, E. D. Dunlop, D. L. Bätzner, A. N. Tiwari, P. Nollet, M. Burgelman, M. Köntges, in *Proceedings of 3rd World Conference on Photovoltaic Energy Conversion*, Osaka **2003**, pp. 356–359; b) X. Sun, T. Silverman, R. Garris, C. Deline, M. A. Alam, *IEEE J. Photovolt.* **2016**, 6, 1298.
- [4] H. Bayhan, E. T. Dağkaldıran, J. D. Major, K. Durose, M. Bayhan, *Semicond. Sci. Technol.* **2019**, 34, 75013.
- [5] M. Barbato, E. Artegiani, M. Bertonecello, M. Meneghini, N. Trivellin, E. Mantoan, A. Romeo, G. Mura, L. Ortolani, E. Zanoni, G. Meneghesso, *J. Phys. D: Appl. Phys.* **2021**, 54, 333002.
- [6] IEC 61215-1-2:2021, *Terrestrial photovoltaic (PV) modules - Design qualification and type approval. Part 1-2: Special requirements for testing of thin-film Cadmium Telluride (CdTe) based photovoltaic (PV) modules* 2021, VDE, Berlin, **2021**, can be found under <https://www.vde-verlag.de/iec-normen/249651/iec-61215-1-2-2021.html>.
- [7] IEC 61215-1-4:2021, *Terrestrial photovoltaic (PV) modules - Design qualification and type approval. Part 1-4: Special requirements for testing of thin-film Cu(In,Ga)(S,Se)<sub>2</sub> based photovoltaic (PV) modules* 2021, VDE, Berlin, **2022**, can be found under <https://www.vde-verlag.de/iec-normen/249686/iec-61215-1-4-2021.html>.
- [8] a) L. Jhamba, D. Wamwangi, Z. Chiguvare, *Opt. Quant. Electron.* **2020**, 52, 245; b) R. Olleao, J. Wang, M. J. Dyson, C. H. L. Weijtens, M. Fattori, B. T. van Gorkom, A. J. J. M. van Breemen, S. C. J. Meskers, R. A. J. Janssen, G. H. Gelinck, *Nat. Commun.* **2021**, 12, 7277.
- [9] a) D. L. King, B. R. Hansen, J. A. Kratochvil, M. A. Quintana in *Conference Record of the Twenty Sixth IEEE Photovoltaic Specialists Conference - 1997*, IEEE, Piscataway, NJ **1997**, pp. 1125; b) S. V. Spataru, D. Sera, P. Hacke, T. Kerekes, R. Teodorescu, *Prog. Photovolt: Res. Appl.* **2016**, 24, 517; c) J. I. Morales-Aragón, M. C. Del Alonso-García, S. Gallardo-Saavedra, V. Alonso-Gómez, J. L. Balenzategui, A. Redondo-Plaza, L. Hernández-Callejo, *Appl. Sci.* **2021**, 11, 1924.
- [10] A. Devasia, S. K. Kurinec, *Am. J. Phys.* **2011**, 79, 1232.
- [11] B. L. Williams, S. Smit, B. J. Kniknie, K. J. Bakker, W. Keuning, W. M. M. Kessels, R. E. I. Schropp, M. Creatore, *Prog. Photovolt: Res. Appl.* **2015**, 23, 1516.
- [12] K. Shen, Q. Li, D. Wang, R. Yang, Y. Deng, M.-J. Jeng, D. Wang, *Sol. Energy Mater. Sol. Cells* **2016**, 144, 472.
- [13] A. Zelenina, F. Werner, H. Elanzeery, M. Melchiorre, S. Siebentritt, *Appl. Phys. Lett.* **2017**, 111, 213903.
- [14] M. Diantoro, T. Suprayogi, A. Hidayat, A. Taufiq, A. Fuad, R. Suryana, *Int. J. Photoenergy* **2018**, 2018, 1.
- [15] S. Dongaonkar, J. D. Servaites, G. M. Ford, S. Loser, J. Moore, R. M. Gelfand, H. Mohseni, H. W. Hillhouse, R. Agrawal, M. A. Ratner, T. J. Marks, M. S. Lundstrom, M. A. Alam, *J. Appl. Phys.* **2010**, 108, 124509.
- [16] a) J. D. Bastidas-Rodríguez, C. A. Ramos-Paja, S. I. Serna-Garcés, *Computation* **2022**, 10, 100; b) A. M. Humada, M. Hojabri, S. Mekhilef, H. M. Hamada, *Renewable Sustainable Energy Rev.* **2016**, 56, 494.
- [17] F. Montalvo-Galicia, M. T. Sanz-Pascual, P. Rosales-Quintero, M. Moreno-Moreno, *Nanomaterials* **2022**, 12, 1955.
- [18] A. Nakane, H. Tampo, M. Tamakoshi, S. Fujimoto, K. M. Kim, S. Kim, H. Shibata, S. Niki, H. Fujiwara, *J. Appl. Phys.* **2016**, 120, 064505.
- [19] S. Gulkowski, A. Zdyb, P. Dragan, *Appl. Sci.* **2019**, 9, 141.
- [20] M. A. Sevillano-Bendezú, M. Khenkin, G. Nofuentes, J. de La Casa, C. Ulbrich, J. A. Töfflinger, *Sol. Energy* **2023**, 259, 174.
- [21] M. A. Scarpulla, B. McCandless, A. B. Phillips, Y. Yan, M. J. Heben, C. Wolden, G. Xiong, W. K. Metzger, D. Mao, D. Krasikov, I. Sankin, S. Grover, A. Munshi, W. Sampath, J. R. Sites, A. Bothwell, D. Albin, M. O. Reese, A. Romeo, M. Nardone, R. Klie, J. Michael Walls, T. Fiducia, A. Abbas, S. M. Hayes, *Sol. Energy Mater. Sol. Cells* **2023**, 255, 112289.
- [22] D. Guo, A. Moore, D. Krasikov, I. Sankin, D. Vasileksa in *2017 IEEE 44th Photovoltaic Specialist Conf. (PVSC)*, IEEE, Piscataway, NJ **2017**, pp. 2816–2818.
- [23] G. Teeter, S. P. Harvey, S. Johnston, *J. Appl. Phys.* **2017**, 121, 043102.
- [24] Y. R. Golive, A. Kottantharayil, J. Vasi, N. Shiradkar, *Prog. Photovolt: Res. Appl.* **2022**, 30, 13.